Evolutionary Pathlines for Blood Flow Exploration
in Cerebral Aneurysms

Benjamin Behrendt, Wito Engelke, Philipp Berg, Oliver Beuing, Bernhard Preim,
Ingrid Hotz, Sylvia Saalfeld

Evolutionary Pathlines for Blood Flow Exploration in Cerebral Aneurysms

B. Behrendt[1] and W. Engelke[2] and P. Berg[3] and O. Beuing[4] and B. Preim[1] and I. Hotz[2] and S. Saalfeld[1]

[1] Department of Simulation and Graphics, University of Magdeburg, Germany
[2] Department of Science and Technology, Linköping University, Sweden
[3] Department of Fluid Dynamics and Technical Flows, University of Magdeburg, Germany
[4] Institute of Neuroradiology, University Hospital Magdeburg, Germany

Abstract

Blood flow simulations play an important role for the understanding of vascular diseases, such as aneurysms. However, analysis of the resulting flow patterns, especially comparisons across patient groups, are challenging. Typically, the hemodynamic analysis relies on trial and error inspection of the flow data based on pathline visualizations and surface renderings. Visualizing too many pathlines at once may obstruct interesting features, e.g., embedded vortices, whereas with too little pathlines, particularities such as flow characteristics in aneurysm blebs might be missed. While filtering and clustering techniques support this task, they require the pre-computation of pathlines densely sampled in the space-time domain. Not only does this become prohibitively expensive for large patient groups, but the results often suffer from undersampling artifacts.
In this work, we propose the usage of evolutionary algorithms to reduce the overhead of computing pathlines that do not contribute to the analysis, while simultaneously reducing the undersampling artifacts. Integrated in an interactive framework, it efficiently supports the evaluation of hemodynamics for clinical research and treatment planning in case of cerebral aneurysms. The specification of general optimization criteria for entire patient groups allows the blood flow data to be batch-processed. We present clinical cases to demonstrate the benefits of our approach especially in presence of aneurysm blebs. Furthermore, we conducted an evaluation with four expert neuroradiologists. As a result, we report advantages of our method for treatment planning to underpin its clinical potential.

CCS Concepts

• ***Human-centered computing*** → *Scientific visualization;*

1. Introduction

The evaluation of blood flow data is increasingly used in medical research to improve the understanding of vascular diseases as well as for treatment planning. An example is the placement of vascular implants to treat aneurysms, which strongly depends on the patient-specific anatomy and hemodynamics. Therefore, flow data is acquired by direct measurement, e.g., using ultrasound or MRI, or generated through simulations using computational fluid dynamics (CFD). In cerebral arteries, blood flow data is mostly obtained by simulations on a subsection of the vessel. Questions relate to the interactions between hemodynamic flow patterns, morphological changes and vascular biology [OJMN*19]. Commonly, blood flow analysis is supported by visualizations based on stream- or pathlines enriched with surface visualizations of the vessel tree. Finding a suitable set of pathlines representing the most important flow patterns while avoiding visual clutter is challenging. A typical solution is to pre-compute sets of lines, commonly generated by dense seeding on a regular 2D grid in the inflow area of the respective vessel

subsection, and then applying filtering. However, the seed points for interesting pathlines are often sparsely distributed in the seeding domain and can therefore easily be missed, even when seeding a high amount of pathlines. Thus, high computational costs are required for pathlines that will never be shown, while still having no guarantee to find the features of interest.

Recently, Engelke et al. introduced evolutionary streamlines for the analysis of steady flows [EH18]. They demonstrate the potential of this method to improve seeding quality and reduce sampling artifacts at significantly reduced computational costs. Additionally, this method does not require a filtering step, since it directly evolves a given set of lines to fulfill specified criteria. In this paper, we propose to extend this method to evolutionary pathlines for unsteady flow analysis in complex vascular domains including pathologies. The generation of feature-sensitive sets of pathlines is integrated in an exploration framework for individual patients as well as the comparison amongst patients. A set of predefined fitness functions supports an automatic extraction of flow patterns of patient groups

with high anatomical variations and aneurysm shapes, including aneurysm blebs or strongly lobulated shapes. 3D visualization of the pathlines gives the anatomical context required for improved treatment planning. Mapping properties of the evolutionary algorithm, such as fitness, onto the pathlines support the comprehensibility of our approach. An easy specification of general optimization criteria for entire patient groups is possible, thus allowing simulated cerebral blood flow data to be batch-processed.

Our method has been technically evaluated with respect to convergence behavior, stability of the results and computational efficiency. A case study shows the usefulness for the analysis of hemodynamic flow in cerebral aneurysms for treatment planning. The feedback of the domain experts suggests that the approach is superior to previous seeding and analysis strategies. The main contributions of our work can be summarized as:

- A new approach for analysis of medical blood flow data based on evolutionary pathlines.
- An efficient pathline seeding strategy to achieve high line coverage, detecting even sparse and highly localized features without relying on a complete field analysis.
- A technical evaluation of the algorithmic properties with respect to convergence, reproducibility, performance and line coverage, as well as an evaluation of the usefulness of the approach with domain experts.

2. Background

Within this section, we provide background information about the application scenario, i.e., cerebral aneurysms, as well as a general introduction to evolutionary algorithms.

2.1. Medical Background

Arteriosclerosis and its accompanying diseases are the leading cause of death in industrialized countries [OJ13]. They may cause cerebral aneurysms — pathologic dilations of the cerebral arterial wall. In case of aneurysm rupture, an ischemic stroke with often fatal consequences for the patient may occur. Especially with respect to increased imaging in the clinical routine, more and more asymptomatical cerebral aneurysms are detected [EBD*13]. Cerebral aneurysms often comprise a daughter aneurysm, also called a *bleb*, which is a prominent bulging on the aneurysm. These blebs are of particular interest, since they have been identified as a factor for increased rupture risk [TMS*05, BRe*03]. Since aneurysm treatment, e.g., endovascular stenting and coiling or neurosurgical clipping, is accompanied with risks for the patient, clinical research aims to avoid unnecessary treatment of incidentally found aneurysms and to identify the best possible treatment with respect to patient-specific anatomy and blood flow behavior.

For rupture risk assessment, clinical risk factors have been identified, e.g., the patient's age, hypertension, aneurysm size and location [GWBJ*14]. State-of-the-art rupture risk models combine morphological parameters characterizing the aneurysm's shape as well as hemodynamical parameters extracted from simulated blood flow to provide further information about the patient-specific risk [DCM*18]. The simulated blood flow not only allows for the
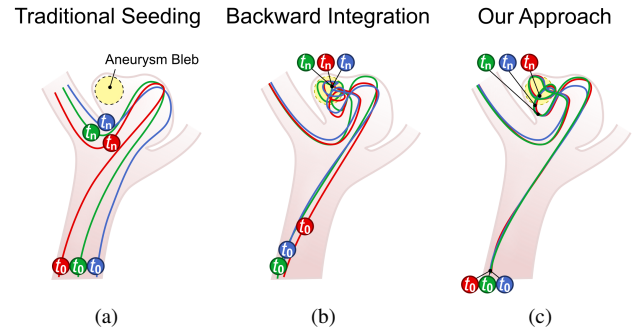
Figure 1: *Illustration of line coverage using different seeding methods. Traditional Seeding (a) is under-sampling the aneurysm bleb. Backward Integration (b) leads to incorrect vortices due to large temporal differences. In contrast, our method (c) generates pathlines with identical start times and reveals complex vortices when searching for pathlines passing a specific area on the vessel surface.*

extraction of flow patterns, but for the extraction of parameters related to pressure and stress as well, e.g., the wall shear stress (WSS), describing the friction of the blood flow on the aneurysm surface, or the oscillatory shear index (OSI), characterizing the variation of the WSS vector over the course of the heart cycle.

For endovascular treatment support, clinical researchers are strongly interested in predicting flow characteristics before and after treatment. Hence, the flow patterns and parameters provide valuable information about the intra-aneurysmal flow [MTXS14]. Implant placement typically aims at aneurysm occlusion, a redirection of the blood flow causing the aneurysm as well as a stabilization of the blood supply of the vessel harboring the aneurysm and its outlets. Virtual implant placement can support the clinician by predicting the resulting blood flow [XDL*15, BSJ*18].

For the blood flow analysis, commercial software, e.g., Star-CCM+ V13.04 (Siemens Product Lifecycle Management Software Inc., Plano, TX, USA 75024), or research tools, e.g., ParaView [AGL05], provide pathline visualizations extracted from the CFD vector field. However, for pathline visualization, even a dense seeding at the parent vessel's inlet or the ostium cannot ensure to entirely represent the intraaneurysmal flow, whereas further increasing the amount of pathlines yields visual clutter. A characterization of blood flow patterns [CCB*05] as well as an aggregation into meaningful clusters [OJCJP16] prevent visual clutter, but depend on pre-integrated lines and cannot account for strongly lobulated aneurysm shapes with blebs. Seeding directly in the region of interest and then performing both forward- and backward-integration generates pathlines in the desired region. However, these pathlines arrive at the inflow plane at different points in time (Fig. 1), which does not accurately represent the blood flow in the vessel and does not meet the requirements of the clinicians. In fact, it could prevent the extraction of complex structures like an embedded vortex. A similar problem arises when using two-pass integration, where potentially interesting seed points for forward-

integration are determined by using backward-integration, as seeding at a different time point (t_0) will produce a different pathline.

2.2. Evolutionary Algorithms

Evolutionary algorithms as meta heuristic for a guided search are based on the principle of natural selection by Charles Darwin [Dar59]. They iteratively improve initial random candidates by using evolution-motivated mechanisms such as *selection*, *crossover* and *mutation*. Thus, a problem of the form:

$$\mathcal{H} = \{x \in \Omega | \forall x' \in \Omega : f(x) \succeq f(x')\}$$

can be optimized, where the goal is to find an element x in the search space Ω which optimizes a function $f : \Omega \to \mathbb{R}$ in Ω. This function is referred to as the *fitness function* and defines a quality measure for the candidate solutions and a comparison operator $\succeq$ in Ω. Furthermore, the specific implementation of the fitness function, selection, and especially the genetic operators (i.e., crossover and mutation) are highly problem-specific. Additional parameters for steering the algorithm are *population size*, *crossover probability*, *mutation probability*, and *mutation strength*.

NOTATION: Throughout this paper, we will use the following notation. We refer to a single solution candidate as *individual I*. The fitness of a specific individual I_i is referred to as $f(I_i)$. Furthermore, a *population P* consists of n_p individuals. Parameters for steering the evolutionary algorithms are percentages for *Elite Selection p_e*, *Mutation p_m*, *Crossover p_c*, and *Insertion p_i*. A single iteration of the evolutionary algorithm is referred to as a *generation*.

INITIALIZATION: In this step, the population P of size n_p is created, with each individual $I \in P$ representing one solution. The initial population contains only individuals with random genomes.

EVALUATION: During the evaluation, each individual's fitness is calculated. With this, we obtain a value $f(I_i)$ with $i \in [0 \dots n_p - 1]$.

FITNESS-BASED SORTING: After evaluation, the list of individuals is sorted according to their fitness. Subsequent steps, such as elite selection, mutation, crossover, and the calculation of convergence measures, rely on an ordered list of individuals.

ELITE SELECTION: This step ensures that good solution candidates are kept between generations. Transferring n_e unmodified individuals to the next generation P' is referred to as elite selection. These individuals are selected from the ordered list according to I_i with $i \in [0 \dots n_e - 1]$ and $n_e = p_e \cdot n_p$.

CROSSOVER: The first genetic operator combines the genome of n individuals to create n offsprings. In its simplest form, with $n = 2$, each offspring inherits half of each parents' genetic information.

MUTATION: The second genetic operator slightly alters each individual's genome, whereas the probability, type and strength of mutation are configurable. This step can be understood as exploration of the local surrounding of a solution candidate in the search space Ω. A mutation is only imposed in subsequent generations if it is beneficial for the individual's fitness. Individuals are selected from an ordered list according to I_i with $i \in [n_c \dots n_e - 1]$ and $n_c = p_c \cdot n_p$, $n_e = p_e \cdot n_p$

INSERTION: This step replaces a part of the population. For this, the $p_i \cdot n_p$ individuals in P with the lowest fitness are replaced by new individuals when inserted in P'. Similar to the initialization, the new individual's genome is randomly generated. This step adds to the genetic diversity and thus ensures further random exploration of the whole search space.

3. Related Work

Geometry-based techniques extracting explicit geometry, e.g., integral or vortex-core lines, are the most frequently used methods for flow analysis [MLP*10]. The biggest challenge of these methods is to avoid clutter and occlusion without missing important features in the data. Typically, these issues are targeted by direct feature extraction, e.g., vortices [KRH*16, KZHH12] or filtering large sets of pre-computed lines. Filtering methods can be divided into two groups. *Explicit filtering* removes lines not satisfying a selected criterion, e.g., defined by line predicates [SGSM08], or using view-dependent criteria based on entropy [LMSC11]. *Implicit filtering* facilitates rendering techniques to emphasize lines of interest while keeping all lines. One example is the work by Günther et al. [GRT14], where line transparency is optimized with respect to an importance criterion. Both approaches discard or hide a high percentage of the calculated lines, which is unfavorable in cases where the line integration is expensive. A second challenge for such methods is to find all interesting features, which cannot be guaranteed even with highly dense sampling.

While all flow visualization techniques are generally applicable, medical flow data has unique requirements. In medical flow visualization, both laminar flow and the vessel surface, which is important for anatomical context information, may occlude interesting, nested flow patterns. Therefore, a variety of methods have been designed specifically for medical applications. A lens metaphor was used by Gasteiger et al. as a screen-space filtering technique that blends between different visualizations on demand [GNBP11]. This allows for clipping parts of the vessel surface to reveal underlying flow structures. However, this method is limited to the examination of local features. Automatic cut-aways for simultaneous visualization of wall parameters and blood flow were introduced by Lawonn et al. [LGV*16]. They additionally use animation for clutter reduction. With this, only small parts of the lines are visible at the same time. Oeltze et al. use streamline clustering based on geometric attributes and cluster representatives to reduce clutter [OLK*14]. Later, they proposed a similar approach to detect embedded vortical flow in cerebral aneurysms [OJCJP16]. Another efficient clustering approach for blood flow data using coherent structures was presented by Englund et al. [ERH16]. Meuschke et al. map the aneurysm surface and pathline cluster representatives to a hemisphere in order to perform an automatic classification of the flow patterns [MOJB*19].

While clustering-based methods are well suited to give an overview of flow, they are less suitable to probe specific flow behavior. Targeting specific medically relevant flow patterns, Neugebauer et al. used the ostium as a seeding plane for pathlines, highlighting the flow entering and leaving an aneurysm [NJB*11]. Behrendt et al. filtered pathlines based on user-selected regions on the vessel surface [BBB*18]. The region selection could be performed either manually or based on static surface parameters, disregarding the temporal dimension of the underlying data. Additionally, the need to perform manual selections on the vessel surface makes this approach time-consuming for larger patient databases.

The aforementioned studies rely on pre-integrated pathlines and are therefore limited by the quality of these lines, especially if a specific flow feature is poorly represented in the unfiltered set. Van Pelt et al. placed seed points on user-defined vessel cross-sections to extract global patterns, such as splitting flow [vBB*10]. The application also offers different seeding strategies and templates. However, they cannot be automatically adapted based on features of interest. The authors performed a user study with four cardiologists, who expressed interest in exploring the effects of different seeding strategies, but preferred to only use a single strategy at a time. Broos et al. determined suitable seeding points for pathlines in 4D PC-MRI data based on a transfer function [BHK*16]. This function calculates a probability value for each voxel based on features such as velocity magnitude or the λ_2 criterion indicating vorticity. The calculated probability determines the likelihood for this voxel to be used as a seed point. While sampling the entire space-time domain is appropriate for low-resolution 4D PC-MRI data, it is not feasible for highly resolved simulation data.

Engelke et al. recently introduced evolutionary algorithms for flow visualization [EH18]. They formulated the task of finding representative lines in a steady flow field as an optimization problem, achieving high quality results while requiring significantly fewer line computations as traditional filtering approaches. They also managed to overcome the problem of under-sampling, since the approach is not tied to a predefined sampling resolution. We build upon this work by

- Extending the algorithm to support time-dependent data and produce pathlines instead of streamlines.
- Adapting the fitness function to specific requirements for blood flow analysis in cerebral aneurysms, including the ability to incorporate properties of the vessel surface into the fitness calculation, inspired by Behrendt et al. [BBB*18].
- Embedding this technique into a framework designed to support clinical research and treatment decisions for cerebral aneurysms.

Evolutionary algorithms can be used for optimization problems, where an analytic solution does not exist and an exhausting exploration is not feasible. Application areas for evolutionary algorithms include parameter optimization (e.g., curvature of pipes) [BS93], packing and scheduling problems, and biological modeling. A recent book [KBB*16] discusses evolutionary algorithms in the context of computational intelligence.

A method to automatically highlight expressive structures in flow fields was presented by Engelke et al. [ELPH18]. Its underlying concept, i.e., multiplication and deletion of particles, is based on local flow properties and cannot be transferred to a line-based approach, where the fitness criteria are defined only for an entire line. Esturo et al. presented a method to find globally optimal stream surfaces by utilizing a domain graph [ESRT13]. The approach is tied to a predefined resolution and unable to find solutions not contained in the graph. In general, adaptive methods follow a similar goal as evolutionary approaches by striving to spend most efforts in regions of interest. A good example in the context of flow analysis is the work by Barakat et al., which uses adaptive refinement for an accurate computation of the flow map [BT13]. The exploitation or refinement aspect of this approach is similar to that of evolutionary algorithms, which is facilitated by mutation.
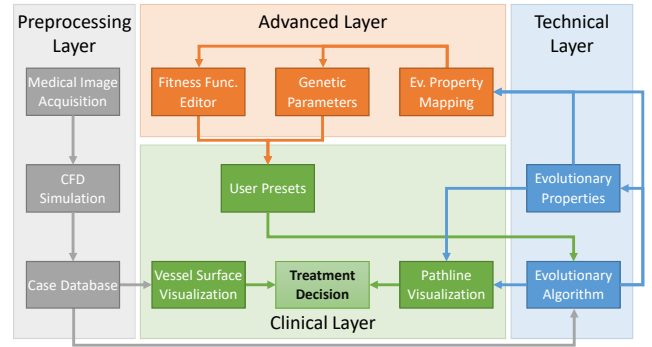
Figure 2: *Overview of the workflows and layers within our framework.*

The exploration aspect differs, as the coverage of adaptive methods is determined in the first step by choosing a base resolution. In contrast, evolutionary algorithms try to achieve good coverage by continuous exploration, which allows them to work with a low population size from the beginning.

4. Evolutionary Aneurysmal Flow Exploration

Within this section we describe our method, consisting of two *Pathline Generation* and *Pathline Visualization*. We start by providing an overview of the associated workflow for different types of users.

4.1. Interaction and Workflow

The visualization and analysis system is composed of three layers: the *Technical Layer* that represents the computational backbone of the system, the *Advanced Layer* targeted at researchers and the *Clinical Layer* targeted at physicians. Additionally, there is a *Preprocessing Layer*, which details the data processing before being imported in our system (Fig. 2).

PREPROCESSING LAYER: Our framework was developed for cerebral aneurysm surface models who are typically extracted from contrast-enhanced 3D rotational angiography. For the cases presented in this work, a threshold-based segmentation approach was applied to the 3D DSA images, followed by marching cubes to obtain a triangulated surface mesh using MeVisLab 2.7 (MeVis Medical Solutions AG, Bremen, Germany) [RBH*11], similar to the approach described in [GBNP15]. For the separation of aneurysm from parent-vessel, we used a semi-automatic neck curve detection [SBN*18]. Based on the segmented aneurysm surfaces, hemodynamic simulations were carried out using STAR-CCM+ 13.04.

TECHNICAL LAYER: This layer contains the main computational components, mainly the evolutionary algorithm with its integrated pathline integrator. It is only targeted towards the developers and maintainers of the system and receives its configuration and data from the other layers.

ADVANCED LAYER: This layer is targeted towards researchers in the medical domain and provides a variety of exploration options. It is designed to support the creation of non-dataset-specific

presets for later use in the clinical layer. Thus, it allows the configuration of the fitness function as well as the genetic parameters for the evolutionary algorithm. The *Fitness Function Editor* enables the user to create a fitness function using a weighted combination of configurable properties, as described in Section 4.2. Similarly, the *Genetic Parameter Editor* allows to configure the parameters for the evolutionary algorithm, such as the mutation rate or number of individuals. The fitness function together with genetic parameters can be saved as a named, dataset-independent preset for specific clinical use cases, e.g., extracting flow structures close to regions with high WSS or OSI. To support comprehensibility of the evolutionary algorithm, it is possible to explicitly filter pathlines in the 3D view based on their overall fitness value. Comprehending why the evolutionary algorithm converges to specific pathline bundles can be a valuable aid in designing fitness functions for later clinical use. For a more in-depth analysis, users may also view the previous generations of pathlines, thus allowing them to trace how the evolutionary algorithm generated the final result. Additionally, the advanced layer also allows to freely configure the pathline visualization with respect to mapping attributes to color scales or opacity, as described in Section 4.3. These settings can also be stored as dataset-independent presets for later clinical use.

CLINICAL LAYER: This layer is reduced to a minimum of interaction, especially tailored to the clinical users and designed to support treatment decisions. It allows for a selection of datasets from the preprocessing layer and presets from the advanced layer. A manual configuration of the fitness function, genetic parameters or visualization settings is not available. Thus, the configuration for a clinical workflow needs to be prepared first within the Advanced Layer. The user can select multiple datasets to perform batch processing with a single preset configuration. Additionally, basic interactions like rotation and zooming in the 3D view are supported.

4.2. Pathline Generation

The input to the evolutionary algorithm is the aneurysm geometry and the simulated blood flow. A plane is automatically fitted in the vessel inlet, which serves as seeding plane for the pathline generation. The evolutionary algorithm details, such as the highly domain-specific encoding of solution candidates and the genetic operators, have been specifically designed for our application.

INDIVIDUALS: The genome of the individuals encodes a single seed point, which uniquely defines a pathline with respect to the integration settings. Thus, the search space Ω is defined by the integral lines' seeding domain. The individuals are stored as two-dimensional points $I_i = (x_i, y_i)$ in the local coordinate system of the seeding plane, with $x_i, y_i \in [0, 1]$. For the integration process, they are transformed into world coordinates. New individuals are always initialized with random values in their genome.

MUTATION: In this step, we add a weighted displacement vector $\mathbf{d} \in [-1.0, 1.0]^d$ to the individual's genome; here, d is the dimension of the search space. Furthermore, we facilitate a generation-dependent weight which decreases with increasing generation count by a constant value, ensuring that with increasing average fitness of the population, solution candidates are altered less.

EVALUATION: To evaluate the fitness of an individual, the entire

pathline has to be integrated from its seed point. We use Shepard interpolation with four samples to acquire the velocity vector from the flow field. The integration is performed with Runge-Kutta-4 (RK4) and a fixed step size of 0.25, although, at the end of the integration, only every fourth point is kept to speed up the visualization and evaluation of the lines. Our collaborating physicians prefer a fixed seeding time to prevent visual confusion from pathlines seeded at different time points being visible simultaneously (recall Figure 1). Furthermore, this better mimics the clinical time-dependent data using contrast agent, which arrives in the vessel as a bolus. Therefore, we always seed at the first time step ($t = 0$). The fitness function $f(I_i)$ is assembled from a set of local properties $f_1..f_n$. The properties can be grouped into two categories:

Line properties produce fitness information based on pathline geometry, such as length or curvature. Both of these measures can indicate the presence of vortex structures, as a pathline is often longer and has higher curvature when passing through a vortex. In cases where a separation of the aneurysm from the parent vessel is available, the residence time of a pathline within the aneurysm can also be used. Thus, only lines in specific regions are favored and thereby implicitly filtered in a spatial manner.

Surface properties produce fitness information based on attributes of the vessel surface close to the pathlines, such as pressure, WSS and OSI. For each vertex of the line, the closest vertex on the surface is efficiently determined using a KD tree. Then, the selected attribute from the surface vertex is normalized and assigned to the pathline vertex as a fitness indicator. Optionally, a distance penalty can be used to reduce the fitness indicator value after a certain distance from the surface to focus on near-wall features.

ANEURYSM GEOMETRY: If the aneurysm in the dataset is segmented, all indicator values for pathline vertices outside a specific region can be disregarded, effectively preventing surface attributes outside of the aneurysm from contributing to the fitness of a line.

$$f_p(I_i) = \bigodot_{j=1}^{|I_i|}(v_{ij}) \tag{1}$$

$$f(I_i) = \sum_{p=1}^{n}(f_p(I_i) \cdot w_p) \tag{2}$$

PATHLINE FITNESS: Each local pathline property $f_p(I_i)$ is assembled from the per-vertex fitness indicators v_{ij}, depending on the number of vertices $|I_i|$ in the line (Eq. 1). Depending on the user configuration, $\odot$ is interpreted as *sum*, *avg* or *max*. Using the sum of the individual indicator values tends to prefer longer lines, as each vertex contributes to the overall fitness even if it has low fitness indicators. Using the average favors short lines, as each vertex with lower fitness indicators reduces the overall line fitness. Using the highest indicator eliminates the length of the line as a fitness factor. The final fitness value for a pathline is the weighted combination of all its pathline properties (Eq. 2). While individual weights (w_p) may be useful and add flexibility for advanced fitness function configurations, we do not explore this aspect and thus use the default value of 1 to weight all pathline properties.

When using a fitness function $f(I_i)$ with respect to multiple sur-

Figure 3: *Different parameter mapping options for pathlines. In (a), the residence time inside the aneurysm is mapped to the opacity and the flow velocity is mapped onto color using a temperature scale (white is slow). In (b), the per-vertex fitness indicator is mapped to color (green-to-red-scale) and the overall line fitness is mapped to thickness.*

face attributes, normalization is important to avoid a bias, as the local fitness values may have different value ranges. Thus, we equalize the value ranges by normalizing all attribute values to the range $[0, 1]$. The user can further constrain this range, e.g., treating all values below or above a given threshold as zero. During the pathline integration, per-vertex fitness indicators and the overall line fitness are stored as attributes and thus are available for exploration and visualization purposes in the *Advanced Layer*.

4.3. Pathline and Context Visualization

Pathlines are visualized as a strip of view-oriented quads inside a semi-transparent vessel model. The opacity of the vessel wall is calculated using a combination of the Fresnel and Phong terms to highlight both the vessel boundaries and the surface shape [GNKP10]. It is possible to map a scalar attribute, such as velocity magnitude or fitness indicators, onto the pathlines (Fig. 3).

5. Results

In this section, we analyze our approach at first with respect to technical quality and performance, and discuss the method from an application point of view.

5.1. Technical Analysis

First, we analyze our evolutionary algorithm with respect to its convergence and reproducibility to evaluate the *Technical Layer* of our workflow. Afterwards, we perform comparisons between our algorithm and a uniform seeding approach regarding the coverage of lines and its performance.

CONVERGENCE: The evolutionary algorithm empirically converges against an ideal result with respect to its fitness function. The convergence speed and the number of iterations needed to reach a sufficiently good result depends on the characteristic behavior of the fitness function within the search domain. There are two main parameters that control the trade-off between the quality of the result and the computation time. These are the population size and the number of generations. To determine a good default value for

the number of generations and the population size, we have run the algorithm on several datasets with different settings and have recorded the fitness values for each generation. Representative values are obtained by averaging the fitness values from ten runs for each population size.

The developments of the maximum fitness and different averages of the best lines are shown in Figure 4 for two datasets. The convergence speed and maximum fitness for the different population sizes is similar in both datasets, suggesting that the population size mainly influences the number of lines the algorithm produces. As a reference, the fitness reached by a uniform seeding approach for 1,000 line computations is plotted. In the first case (Fig. 4(a)), the uniform seeding produces a single line with a higher fitness than all lines generated by the evolutionary algorithm. However, the 10%, 20% and 50% best lines by the evolutionary algorithm exceed those of the uniform seeding approach after only a few iterations. In the second case, the peak fitness value of the evolutionary algorithm soon exceeds the reference values (Fig. 4(b)). After a few additional iterations, even the average fitness of the 10% best lines from the evolutionary algorithm comes close to the fitness of the best uniformly seeded line. This shows that better results as with the standard approach can be achieved even though areas with high fitness values are sparse and localized.

A fitness map shows the projected fitness of each individual on the seed plane for a single run of the evolutionary algorithm (Fig. 5(a)). The projection is achieved by rendering a Voronoi diagram, where each seed point creates a cell that is colored according to the fitness of that point. With the given settings ($n_p = 200$, $p_e = 30\%$, $p_c = 0\%$, $p_m = 30\%$, $p_i = 40\%$), the evolutionary algorithm integrated $8{,}120$ pathlines in total. The map shows that the sampling rate automatically adapts to the fitness function. The resolution of the map is noticeably lower in areas with lower fitness, as the algorithm generally favours the exploration of high-fitness areas. To compare the result with fitness maps created using uniform seeding, we first use the same number of lines (Fig. 5(b)). Then, we increase the number of lines to 10^6 lines to obtain a map that is close to the ground truth (Fig. 5(c)). In regions with lower to medium fitness, the evolutionary algorithm is very close to the comparative run with the same number of lines. In areas with high

(a)

(b)
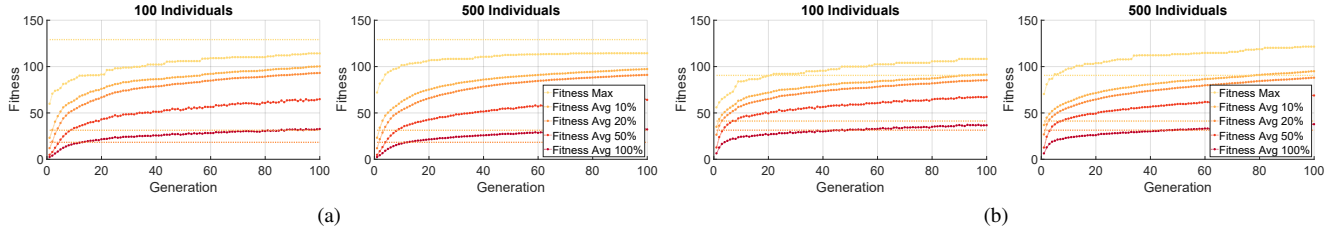
Figure 4: *Average fitness curves (max fitness, top 10%, top 20%, top 50% and all lines) for 10 respective runs on two datasets (a) and (b) with identical configuration ($p_e = 30\%$, $p_c = 0\%$, $p_m = 30\%$, $p_i = 40\%$), but different population sizes (100 and 500). Horizontal lines indicate max fitness, top 10% and top 20% reached with uniform seeding of 1000 lines. Note that the best lines' fitness might be higher with uniform seeding compared to the evolutionary algorithm (see (a)), the averages are far below. Even after a couple of generations the evolutionary algorithm produces more lines with higher fitness than the uniform seeding approach.*


(a)   (b)   (c)
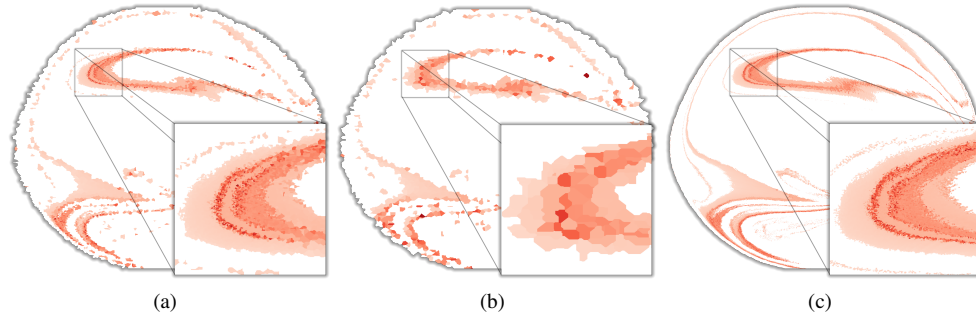
Figure 5: *Fitness map of the seed plane from the evolutionary algorithm and a total of 8120 line computations; (a) and a uniform sampling using the same number of lines (b) and 10^6 lines (c). Darker colors indicate higher fitness values, whereas in white areas the resulting pathline did not pass the aneurysm and therefore no fitness value is assigned. Seeding 10^6 lines takes multiple hours and thus is unfeasible in practical applications, hence uniform seeding approaches would likely miss the isolated and spatially confined maxima on the plane.*

fitness, it is almost identical to the densely sampled map (compare highlighted regions in Figure 5). The fitness values reached by all three approaches are summarized in Table 1. For both uniform sampling computations the fitness values are very similar. Integrating 10^6 lines leads to a better peak fitness due to a more exhaustive sampling of the seeding space. The evolutionary approach reaches nearly the same peak fitness as the dense seeding, despite integrating significantly fewer lines. However, the 10%, 20% and 50% best lines have a significantly higher fitness than both of the uniform approaches.

To understand the influence of the population size on the convergence and thus the total number of lines that have to be computed, we recorded the fitness reached for identical configurations, but different population sizes (Fig. 6). As expected, a greater number of individuals for each generation increases the speed at which the evolutionary algorithm converges, but also increases the computational effort.

(a)
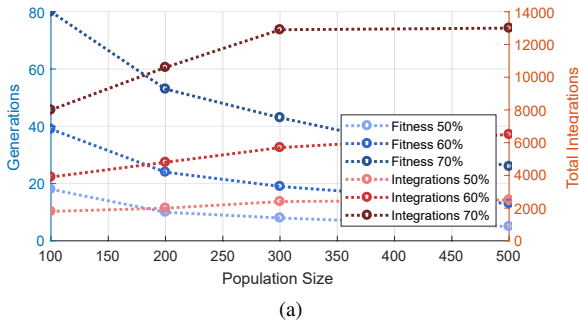
Figure 6: *Varying population size in comparison. Blue graphs show generations needed until the best 25 lines reach 50, 60 and 70% of the maximum fitness, respectively. Red graphs show total the amount of performed line computations.*
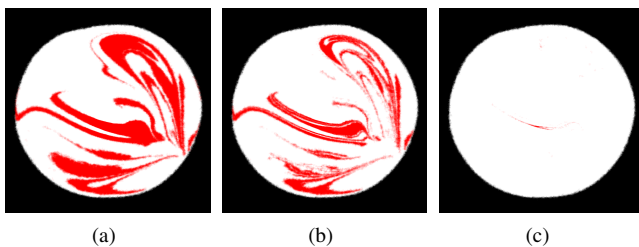
Table 1: *Fitness comparison between our evolutionary approach and uniform seeding with 8,120 and 10^6 pathlines respectively.*

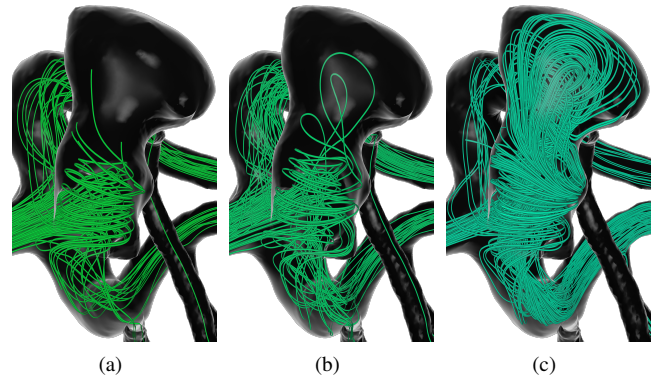|	*Ev. algorithm*	*8,120 lines*	*10^6 lines*
Fitness Max	112.1	113.6	119.1
Fitness Avg. 10%	96.7	60.5	60.3
Fitness Avg. 20%	90.6	51.6	50.9
Fitness Avg. 50%	64	36.4	34.9
Fitness Avg. 100%	32.2	23.4	22.6

(a)　　　　　　　　(b)
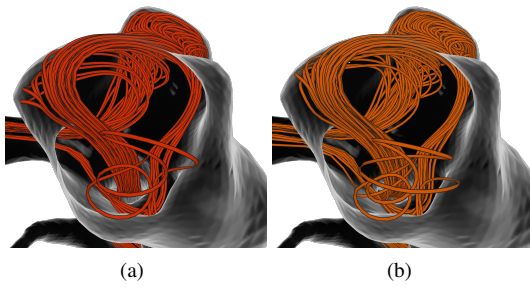
Figure 7: *Pathlines from two evolutionary algorithms using the same configuration, but different random seeds.*

(a)　　　　　(b)　　　　　(c)

Figure 9: *Comparison of expressive line sets for an aneurysm: We compare the output of a uniform seeding approach (using ParaView 5.5.0 (a) and our in-house integrator (b)) with our evolutionary algorithm (c). In both (a) and (b), almost no lines reach the dome and therefore leave it heavily underpopulated, whereas the dome is densely covered in (c).*

REPRODUCIBILITY: Due to the random nature of both the mutation and initialization of new points, two runs of the evolutionary algorithm with identical configuration will generate different line sets. To analyze the sensitivity of the results to this randomness, we performed multiple runs with identical configuration. Visually, the resulting pathline sets are highly similar (Fig. 7). Additionally, we compare the fitness maps from 20 runs with different seed values and highlight regions with a relative fitness above a given threshold. The resulting images are thresholded and used to compute the mean pairwise Sørensen-Dice coefficient (*DC*) using the DC calculator by Tom Lawton [Law17]. DC is a summary measure of spatial overlap to compare the similarity of two binary images, where 0 means no overlap and 1 refers to complete overlap. For regions with a relative fitness above 0 (i.e., the seed regions that produce pathlines entering the aneurysm), the DC reached a value of 0.87. The DC for regions with a relative fitness above 25% and 90% of the maximum reached 0.72 and 0.42, respectively. Visual inspection shows that the differences are mostly located around the edges of the detected regions. Increasing the threshold lowers the overall size of the regions, thus increasing this effect and lowering the DC. Yet, regardless of the threshold, overlaying all 20 fitness maps shows that the detected regions are visually similar (Fig. 8). Thus we can conclude that, despite the variances in the results, the algorithm acts in a predictable and stable way. However, as exact reproducibility may be important in some use cases, our framework exposes the seed value for the random number generator to the user.
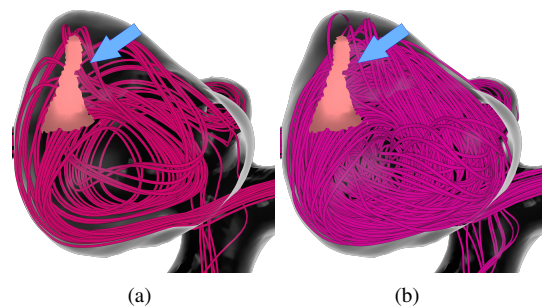
Running the evolutionary algorithm twice with an identical configuration *and* random seed value will always yield identical results.

COVERAGE: Uniform seeding strategies on the inflow plane suffer from poor line-coverage in hard-to-reach parts of the aneurysm, especially in blebs. To demonstrate the ability of our algorithm to reach these areas, we compared it against ParaView (version 5.5.0) as well as our own line integrator using a uniform seeding strategy. In all cases, we seeded 300 individual lines. Both ParaView as well as our application used uniformly distributed seed points at the inlet for the uniform seeding approach. As we were not able to entirely replicate our own integration parameters in ParaView, the resulting lines are slightly different. The evolutionary algorithm was configured with $n_p = 300$, $p_e = 30\%$, $p_c = 0\%$, $p_m = 30\%$, $p_i = 40\%$, using the total length of each line in the aneurysm as its fitness function and iterated over 30 generations. Both uniform seeding approaches produce similar results (Fig. 9(a) and 9(b)), with the top part of the aneurysm nearly entirely empty. The evolutionary

(a)　　　　　(b)　　　　　(c)

Figure 8: *Average projection of the 20 thresholded seed plane fitness maps with the same fitness function, but different random seed values. Thresholds for the relative fitness were set to 0% (a), 25% (b) and 90% (c)*

(a)　　　　　　　　(b)

Figure 10: *Comparison of line coverage using uniform seeding methods (a) and our method (b) when searching for pathlines passing near a specific area on the vessel surface (arrow).*
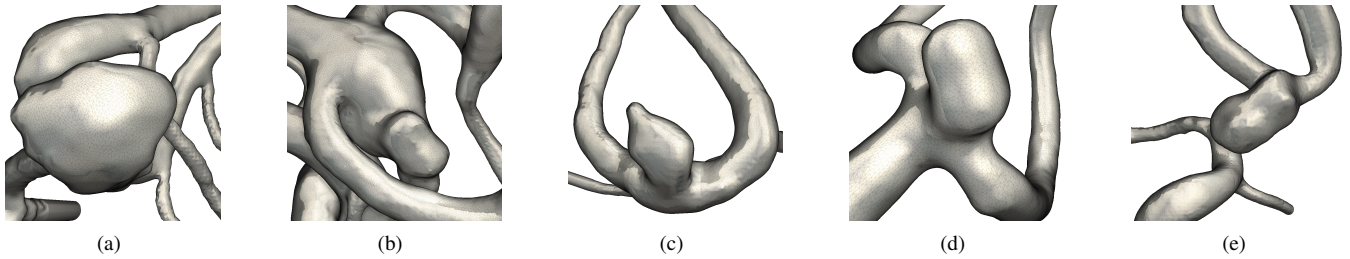
Figure 11: *Selected cases for our evaluation comprising four aneurysms at the anterior communicating artery (Case 1 (a) – male, 36 years; Case 2 (b) – male, 63 years; Case 3 (c) – male, 86 years; Case 5 (e) – female, 38 years) and one at the bifurcating middle cerebral artery aneurysm (Case 4 (d) – female, 59 years).*

seeding, on the other hand, manages to capture the flow in the entire aneurysm (Fig. 9(c)).

PERFORMANCE: The most time-consuming part of the evolutionary algorithm is the evaluation of the fitness function, as it requires the full integration of a pathline and subsequent calculation of the fitness indicators for each pathline vertex. Figure 10 presents a comparison between the result from a uniform seeding approach with subsequent filtering and our evolutionary algorithm using an identical fitness criterion. For the uniform approach, $1,000$ lines were seeded in total, whereas 23 lines remained after filtering (Fig. 10(a)). For the evolutionary approach, 460 lines were seeded in total ($n_p = 100$, $p_e = 30\%$, $p_c = 0\%$, $p_m = 30\%$, $p_i = 40\%$) over ten generations and the best 47 lines were used (Fig. 10(b)). 53 lines with a fitness value of 0 were discarded. Despite seeding less than half of the amount of lines than with the uniform approach, the evolutionary algorithm produces a denser set of lines fulfilling the criterion. Integrating the 1000 lines using the uniform approach took 53 seconds (without performing filtering) on an *Intel i5-6500* with four cores clocked at 3.2 GHz, whereas the evolutionary algorithm took 45 seconds (including the evaluation of the fitness function). Integrating and evaluating pathlines to computing the densely seeded map from Figure 5(c) took eight hours. Since only small areas on the seeding plane result in lines with a high fitness value (Fig. 5), the uniform seeding approach struggles to position a sufficient amount of seed points in these areas without strongly oversampling areas with lower fitness. Based on the results (Fig. 6), we concluded that a population size of 200 or 300 is the best trade-off between fast convergence, total amount of line computations including evaluation and run stability, i.e., less variations between runs with different random seeds. While a population size of 100 also provides reasonable convergence speed and stability, the total amount of generated lines may be insufficient to facilitate a dense 3D visualization.

5.2. Expert Feedback

We performed a general evaluation with an experienced neuroradiologist (*Physician A*), who was also involved in the design process of our framework. Afterwards, we conducted a more specific evaluation of the *Clinical Layer* of our workflow with three additional neuroradiologists (*Physician B*, *Physician C* and *Physician D*), who were not familiar with our tool, to validate its clinical use-

fulness with respect to treatment planning. As suggested by Preim et. al, such a procedure is crucial to achieve meaningful evaluation results [PRI18]. Our goal was to evaluate

1. which fitness function configuration produces the most satisfactory line bundles for this purpose.
2. whether the visualization of hemodynamic information using evolutionary pathlines influences the treatment decision.

To answer question 1, we asked *Physician A* to compare the resulting lines of different fitness functions. The comparison consisted of pathlines optimized for length and to pass by surface areas in the aneurysm with high and low wall shear stress (WSS) as well as high and low oscillatory shear index (OSI). The physician was able to easily identify differences between line bundles optimized with respect to high or low OSI. Interestingly, he was able to infer the location of high and low OSI or WSS values on the surface by comparing their respective line bundles. To evaluate the blood flow for treatment decisions, he preferred the length-based fitness function, as it ensured that the entire aneurysm was filled with pathlines. He did not find significant differences in the pathline bundles created using the OSI-based fitness function in comparison to the WSS-based fitness function. This could be explained with the fact that the OSI is derived from the WSS. Therefore both attributes lead to similar line bundles.

In clinical practice, the placement of stents with or without coiling to treat aneurysms is decided based on the patient-specific anatomy. To assess a benefit in treatment planning, we had to identify well suited test cases first. Therefore, we conducted a quick survey of a database containing more than 100 cerebral aneurysms with *Physician A*, who had been treating these patients. We selected five cases with a challenging anatomy, i.e., aneurysms that are located at bifurcations with almost symmetrical outlet configurations (Fig. 11). To answer question 2, we presented the other experts (*Physician B-D*) with these five cases. They varied with respect to their work experience of endovascular treatment, including the hospital director (20 years of neurointerventional experience), a senior physician (9 years) and a novice physician (1 year). They were blinded to the applied treatment and patient outcome, but provided with clinical information such as the patients' sex and age.

The first visualization only depicted the vessel surface without any hemodynamic information. The physicians were asked about their treatment decision based on the given visualization. After-

Table 2: *Results of our evaluation for physicians B, C and D, when only seeing the 3D view for anatomical information (before) and after seeing our pathline visualization (after). Treatment decisions were: stent-assisted coiling (C & S), y-stenting (Y–S), i.e., implanting two stents, and coiling without stenting (C). Changes in treatment decisions are highlighted via color-coding.*

	Physician B	Physician C	Physician D
Case 1 - before	C & S	C & S	Y – S
Case 1 - after	C & S	C & S	C & S
Case 2 - before	Y – S	C & S	Y – S
Case 2 - after	Y – S	C & S	Y – S
Case 3 - before	C	C & S	Y – S
Case 3 - after	C	Y – S	C & S
Case 4 - before	Y – S	C & S	Y – S
Case 4 - after	Y – S	Y – S	Y – S
Case 5 - before	Y – S	C & S	Y – S
Case 5 - after	Y – S	Y – S	Y – S

wards, we presented them with the same dataset using our visualization techniques, including pathlines extracted by the evolutionary algorithm, and asked whether they would revise their decision. In both cases, they had full control of the viewing direction. For this evaluation, we chose a fitness function based on both line length and residence time of the flow inside the aneurysm, as it achieves a pathline coverage superior to uniform seeding approaches and covers the whole aneurysm. The results are provided in Table 2.

In four of five cases, at least one physician changed his or her treatment decision after exploring our evolutionary pathlines. These changes were motivated by an improved understanding of the intra-aneurysmal flow and its splitting into the outlets, including flow patterns. In three cases, these changes lead to more consistency in the final decision between the physicians. The third aneurysm was the most challenging one, as two physicians changed their minds and the final decisions are not consistent between them. On the one hand, their initial decisions were similarly inconsistent, but on the other hand, we selected challenging cases. Interestingly, the most experienced physician never changed his mind.

6. Discussion and Conclusion

We presented an adaption of the recently developed evolutionary lines to the medical domain by carefully adjusting the genetic operators to fit clinical and research requirements. We showed the usefulness of an evolutionary algorithm for seeding pathlines in cerebral blood flow data. Our approach shows significant improvements over existing seeding strategies, both in terms of computational effort and quality of results. Better coverage of hemodynamically interesting regions, such as aneurysm domes or blebs, is the major advantage over previous work. Thus, flow patterns can be identified in a more reproducible manner, which is essential to assessing the aneurysm rupture risk.

We mainly examined the feasibility of using evolutionary lines to visualize hemodynamics in cerebral aneurysms. The design of our fitness functions is tailored towards the examination of simulated blood flow in cerebral aneurysms, but could also be adapted

to fulfil the specific research requirements for other blood vessels or data acquisition methods. An interesting extension would be the introduction of a normalization between the fitness value ranges of surface and pathline properties, in order to allow more combinations of properties and thus increase the flexibility of the fitness function. Further improvements, especially with respect to the conversion speed, could be achieved by an in-depth analysis of the parameter space of the genetic operators.

Currently, each individual in our evolutionary algorithm represents a single pathline. For the future, we plan to support additional types of structures, such as streaklines or line bundles. The evolutionary algorithm treats and optimizes each individual as a separate entity, therefore increasing the fitness of singular lines, but not guaranteeing diversity between the resulting lines. By using line bundles instead of singular lines as individuals, the coverage within the aneurysm could be further improved. A different solution to this problem could be the usage of seed plane fitness maps, which are generated as a side-product of the evolutionary algorithm, for a final seeding step.

References

[AGL05] AHRENS J., GEVECI B., LAW C.: Paraview: An end-user tool for large data visualization. *The visualization handbook 717* (2005). 2

[BBB*18] BEHRENDT B., BERG P., BEUING O., PREIM B., SAALFELD S.: Explorative blood flow visualization using dynamic line filtering based on surface features. *Comput Graph Forum 37*, 3 (2018), 183–194. 3, 4

[BHK*16] BROOS A. J. M., HOON, NIELS H. L. C. DE, KONING, PATRICK J. H. DE, GEEST, ROB J. VAN DER, VILANOVA A., JALBA A. C.: A framework for fast initial exploration of PC-MRI cardiac flow. In *Proc. of the EG workshop on Visual Computing for Biology and Medicine (VCBM)* (2016), pp. 69–78. 4

[BRe*03] BECK J., ROHDE S., EL BELTAGY M., ZIMMERMANN M., BERKEFELD J., SEIFERT V., ET AL.: Difference in configuration of ruptured and unruptured intracranial aneurysms determined by biplanar digital subtraction angiography. *Acta neurochirurgica 145*, 10 (2003), 861–5; discussion 865. 2

[BS93] BÄCK T., SCHWEFEL H.-P.: An overview of evolutionary algorithms for parameter optimization. *Evolutionary computation 1*, 1 (1993), 1–23. 4

[BSJ*18] BERG P., SAALFELD S., JANIGA G., BRINA O., CANCELLIERE N. M., MACHI P., ET AL.: Virtual stenting of intracranial aneurysms: A pilot study for the prediction of treatment success based on hemodynamic simulations. *The International Journal of Artificial Organs 41*, 11 (2018), 698–705. 2

[BT13] BARAKAT S. S., TRICOCHE X.: Adaptive refinement of the flow map using sparse samples. *IEEE Trans Vis Comput Graph 19*, 12 (2013), 2753–2762. 4

[CCB*05] CEBRAL J. R., CASTRO M. A., BURGESS J. E., PERGOLIZZI R. S., SHERIDAN M. J., PUTMAN C. M.: Characterization of cerebral aneurysms for assessing risk of rupture by using patient-specific computational hemodynamics models. *American Journal of Neuroradiology 26*, 10 (2005), 2550–2559. 2

[Dar59] DARWIN C.: *The Origin of Species by means of Natural Selection, or, the Preservation of Favoured Races in the struggle for life*. John Murray, 1859. 3

[DCM*18] DETMER F. J., CHUNG B. J., MUT F., SLAWSKI M., HAMZEI-SICHANI F., PUTMAN C., ET AL.: Development and internal validation of an aneurysm rupture probability model based on patient characteristics and aneurysm location, morphology, and hemodynamics. *International Journal of Computer Assisted Radiology and Surgery 13*, 11 (2018), 1767–1779. 2

[EBD*13] ETMINAN N., BUCHHOLZ B. A., DREIER R., BRUCKNER P., TORNER J. C., STEIGER H.-J., ET AL.: Cerebral aneurysms: Formation, progression and developmental chronology. *Translational stroke research 5*, 2 (2013), 167–173. 2

[EH18] ENGELKE W., HOTZ I.: Evolutionary Lines for Flow Visualization. In *EuroVis 2018 - Short Papers* (2018). 1, 4

[ELPH18] ENGELKE W., LAWONN K., PREIM B., HOTZ I.: Autonomous Particles for Interactive Flow Visualization. *Comput Graph Forum 38*, 1 (2018), 248–259. 4

[ERH16] ENGLUND R., ROPINSKI T., HOTZ I.: Coherence maps for blood flow exploration. In *Proc. of the EG workshop on Visual Computing for Biology and Medicine (VCBM)* (2016), pp. 79–88. 3

[ESRT13] ESTURO J. M., SCHULZE M., RÖSSL C., THEISEL H.: Global selection of stream surfaces. *Comput Graph Forum 32*, 2pt1 (2013), 113–122. 4

[GBNP15] GLASSER S., BERG P., NEUGEBAUER M., PREIM B.: Reconstruction of 3D Surface Meshes for Bood Flow Simulations of Intracranial Aneurysms. In *Proc. of computer- and roboter-assisted surgery (CURAC)* (2015), pp. 163–168. 4

[GNBP11] GASTEIGER R., NEUGEBAUER M., BEUING O., PREIM B.: The FLOWLENS: A focus-and-context visualization approach for exploration of blood flow in cerebral aneurysms. *IEEE Trans Vis Comput Graph 17*, 12 (2011), 2183–2192. 3

[GNKP10] GASTEIGER R., NEUGEBAUER M., KUBISCH C., PREIM B.: Adapted Surface Visualization of Cerebral Aneurysms with Embedded Blood Flow Information. In *Proc. of the EG workshop on Visual Computing for Biology and Medicine (VCBM)* (2010), pp. 25–32. 6

[GRT14] GÜNTHER T., RÖSSL C., THEISEL H.: Hierarchical opacity optimization for sets of 3d line fields. *Comput Graph Forum 33*, 2 (2014), 507–516. 3

[GWBJ*14] GREVING J. P., WERMER M. J., BROWN JR R. D., MORITA A., JUVELA S., YONEKURA M., ET AL.: Development of the phases score for prediction of risk of rupture of intracranial aneurysms: a pooled analysis of six prospective cohort studies. *The Lancet Neurology 13*, 1 (2014), 59–66. 2

[KBB*16] KRUSE R., BORGELT C., BRAUNE C., MOSTAGHIM S., STEINBRECHER M.: *Computational Intelligence: A Methodological Introduction, 2nd Edition*. Springer, New York, 2016. 4

[KRH*16] KASTEN J., REININGHAUS J., HOTZ I., HEGE H.-C., NOACK B. R., DAVILLER G., ET AL.: Acceleration feature points of unsteady shear flows. *Archives of Mechanics 68*, 1 (2016), 55–80. 3

[KZHH12] KASTEN J., ZOUFAHL A., HEGE H. C., HOTZ I.: Analysis of vortex merge graphs. In *Proc. of Vision, Modeling, and Visualization* (2012). 3

[Law17] LAWTON T.: DSCImageCalc v1.2a, 2017. 8

[LGV*16] LAWONN K., GLASSER S., VILANOVA A., PREIM B., ISENBERG T.: Occlusion-free Blood Flow Animation with Wall Thickness Visualization. *IEEE Trans Vis Comput Graph 22*, 1 (2016), 728–737. 3

[LMSC11] LEE T.-Y., MISHCHENKO O., SHEN H.-W., CRAWFIS R.: View point evaluation and streamline filtering for flow visualization. In *Proc. of IEEE PacificVIS* (2011), pp. 83–90. 3

[MLP*10] MCLOUGHLIN T., LARAMEE R. S., PEIKERT R., CHEN M., POST F. H., CHEN M.: Over two decades of integration-based, geometric flow visualization. *Comput Graph Forum 29*, 6 (2010), 1807–1829. 3

[MOJB*19] MEUSCHKE M., OELTZE-JAFRA S., BEUING O., PREIM B., LAWONN K.: Classification of Blood Flow Patterns in Cerebral Aneurysms. *IEEE Trans Vis Comput Graph 25*, 7 (2019), 2404–2418. 3

[MTXS14] MENG H., TUTINO V. M., XIANG J., SIDDIQUI A.: High WSS or low WSS? Complex interactions of hemodynamics with intracranial aneurysm initiation, growth, and rupture: toward a unifying hypothesis. *American Journal of Neuroradiology 35*, 7 (2014), 1254–62. 2

[NJB*11] NEUGEBAUER M., JANIGA G., BEUING O., SKALEJ M., PREIM B.: Anatomy-Guided Multi-Level Exploration of Blood Flow in Cerebral Aneurysms. *Comput Graph Forum 30*, 3 (2011), 1041–1050. 3

[OJ13] OSBORN E. A., JAFFER F. A.: Imaging atherosclerosis and risk of plaque rupture. *Current Atherosclerosis Reports 15*, 10 (2013), 359. 2

[OJCJP16] OELTZE-JAFRA S., CEBRAL J. R., JANIGA G., PREIM B.: Cluster Analysis of Vortical Flow in Simulations of Cerebral Aneurysm Hemodynamics. *IEEE Trans Vis Comput Graph 22*, 1 (2016), 757–766. 2, 3

[OJMN*19] OELTZE-JAFRA S., MEUSCHKE M., NEUGEBAUER M., SAALFELD S., LAWONN K., JANIGA G., ET AL.: Generation and visual exploration of medical flow data: Survey, research trends and future challenges. *Comput Graph Forum 40*, 4 (2019), 860. 1

[OLK*14] OELTZE S., LEHMANN D. J., KUHN A., JANIGA G., THEISEL H., PREIM B.: Blood Flow Clustering and Applications in Virtual Stenting of Intracranial Aneurysms. *IEEE Trans Vis Comput Graph 20*, 5 (2014), 686–701. 3

[PRI18] PREIM B., ROPINSKI T., ISENBERG P.: A Critical Analysis of the Evaluation Practice in Medical Visualization. In *Proc. of the EG workshop on Visual Computing for Biology and Medicine (VCBM)* (2018), pp. 45–56. 9

[RBH*11] RITTER F., BOSKAMP T., HOMEYER A., LAUE H., SCHWIER M., LINK F., ET AL.: Medical image analysis. *IEEE pulse 2*, 6 (2011), 60–70. 4

[SBN*18] SAALFELD S., BERG P., NIEMANN A., LUZ M., PREIM B., BEUING O.: Semiautomatic neck curve reconstruction for intracranial aneurysm rupture risk assessment based on morphological parameters. *International journal of computer assisted radiology and surgery 13*, 11 (2018), 1781–1793. 4

[SGSM08] SALZBRUNN T., GARTH C., SCHEUERMANN G., MEYER J.: Pathline predicates and unsteady flow structures. *The Visual Computer 24*, 12 (2008), 1039–1051. 3

[TMS*05] TSUKAHARA T., MURAKAMI N., SAKURAI Y., YONEKURA M., TAKAHASHI T., INOUE T., ET AL.: Treatment of unruptured cerebral aneurysms; a multi-center study at Japanese national hospitals. In *New Trends of Surgery for Stroke and its Perioperative Management*, vol. 94 of *Acta Neurochirurgica Supplements*. 2005, pp. 77–85. 2

[vBB*10] VAN PELT R., BESCÓS J. O., BREEUWER M., CLOUGH R. E., GRÖLLER M. E., TER HAAR ROMENIJ B., ET AL.: Exploration of 4D MRI Blood Flow using Stylistic Visualization. *IEEE Trans Vis Comput Graph 16*, 6 (2010), 1339–1347. 4

[XDL*15] XIANG J., DAMIANO R. J., LIN N., SNYDER K. V., SIDDIQUI A. H., LEVY E. I., ET AL.: High-fidelity virtual stenting: modeling of flow diverter deployment for hemodynamic characterization of complex intracranial aneurysms. *Journal of Neurosurgery 123*, 4 (2015), 832–840. 2